SCIENTIFIC REPORTS

OPEN

Photoinduced Charge Transport in a BHJ Solar Cell Controlled by an External Electric Field

Received: 08 January 2015
Accepted: 12 August 2015
Published: 10 September 2015

Yongqing Li[1,3], Yanting Feng[1,2] & Mengtao Sun[1,2]

This study investigated theoretical photoinduced charge transport in a bulk heterojunction (BHJ) solar cell controlled by an external electric field. Our method for visualizing charge difference density identified the excited state properties of photoinduced charge transfer, and the charge transfer excited states were distinguished from local excited states during electronic transitions. Furthermore, the calculated rates for the charge transfer revealed that the charge transfer was strongly influenced by the external electric field. The external electric field accelerated the rate of charge transfer by up to one order when charge recombination was significantly restrained. Our research demonstrated that photoinduced charge transport controlled by an external electric field in a BHJ solar cell is efficient, and *the exciton dissociation is not the limiting factor in organic solar cells*. Our research should aid in the rational design of a novel conjugated system of organic solar cells.

Organic solar cells are a rapidly developing novel technology with environmental and economic[1–3] advantages. Organic solar cells can be grouped into small organic molecule cells and polymer cells, the latter of which are a popular research area. A significant number of experimental and theoretical investigations have been performed to improve the photoelectric transformation efficiency of bulk heterojunction polymer solar cells. Donors and acceptors are important carriers in photoelectric transformation, and these carriers determine the photoelectric transformation efficiency[4,5]. Under light, electron-hole pairs can be created in donors. Under the influence of a built-in electric field, the electron-hole pairs separate and are transferred to the electrodes, where they are collected. In electric charge transfer, the electrons move to the cathode, while the holes move to the anode. Theoretical calculations play an important role in studying the relationship between the optical properties and the chemical structures of electronic donors and acceptors. Theoretical calculations are also critical for designing a novel and feasible donor-acceptor system. From the electronic structure perspective, donors and acceptors have a strong electronic coupling effect, which results in a low exciton binding energy. Quantum calculations can provide important information for the study of the photoinduced electric charge transfer mechanism in a donor-acceptor system. Recently, many organic solar cell materials with high photoelectric transformation efficiencies have been created, such as PCDPTBT/$PC_{61}BT$[6], $PTB_7/PC_{71}BM$[7], PBDTT-DPP/$PC_{61}BM$ and PCPDT-BT/$PC_{71}BM$[8,9], for which the photoelectric transformation efficiencies are 6.7%, 7.4%, 8.6% and 10.6%, respectively.

Electric charge transfer theory has developed rapidly since the electric charge transfer phenomenon was first discovered in the 1930s[10]. In 1956, Marcus and colleagues created a unified understanding of electric charge transfer theory and predicted the existence of the inverted region[11]. Later, the existence of the inverted region was demonstrated experimentally by Miller and Closs[12]. Because of its low bandgap, which can effectively increase light absorption, a BT-$PC_{61}BM$ molecule system was chosen for our calculations. In this paper, the photoinduced charge transfer rate and energy transfer mechanism of a BT-$PC_{61}BM$ molecule system were studied based on Marcus theory. We visualized the process of charge

[1]Department of Physics, Liaoning University, Shenyang 110036, P. R. China. [2]Beijing National Laboratory for Condensed Matter Physics, Institute of Physics, Chinese Academy of Science, P. O. Box 603-146, Beijing, 100190, P. R. China. [3]State Key Lab of Molecular Reaction Dynamics, Dalian Institute of Chemical Physics, Chinese Academy of Sciences, Dalian 116023, China. Correspondence and requests for materials should be addressed to Y.L. (email: yqli@lnu.edu.cn) or M.S. (email: mtsun@iphy.ac.cn)

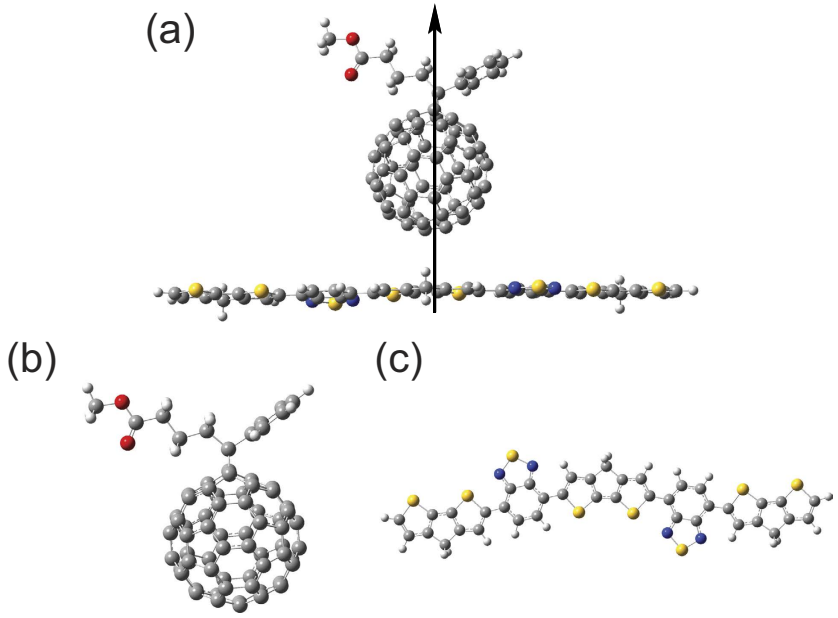

Figure 1. Chemical structure of the BT: $PC_{61}BM$ blend **(a)**, $PC_{61}BM$ **(b)** and BT **(c).** The electric field is oriented along the coordinate.

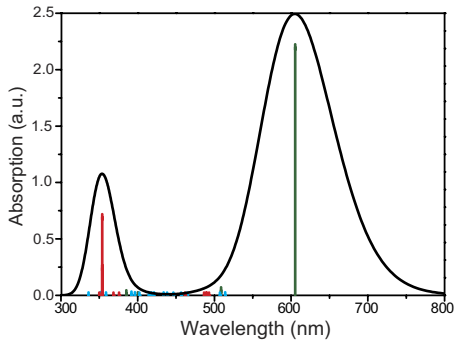

Figure 2. Optical electronic state absorption spectra of BT-$PC_{61}BM$, in which the green line, red line and blue line denote LE(BT), ICT and LE($PC_{61}BM$), respectively.

transfer using three-dimensional (3D) visualization technologies and uncovered the charge transfer and energy transfer mechanism of the optical functional materials[13–17].

Results

Properties of the excitation state. A C_{60} molecule, also known as a buckyball, consists of 60 carbon atoms and has a good electron affinity. A BT molecule (see Fig. 1), with an absorption region ranging from 300 to 800 nm, mainly consists of methine (=CH-). Owing to its broad spectral response range, a BT molecule has a strong ability to capture light. In this study, we combined a BT molecule and a $PC_{61}BM$ molecule to investigate the properties of a BT-$PC_{61}BM$ molecular complex in an excited state.

To simulate the optical properties of a BT-$PC_{61}BM$ molecule, the excited state electronic transitions were calculated using the time-dependent density functional theory (TDDFT) method, and a long-range-corrected functional (CAM-B3LYP) was employed for the non-Coulombic part of the exchange functional. The relevant results for the calculated absorption spectroscopy of the BT-$PC_{61}BM$ molecule are shown in Fig. 2. The BT-$PC_{61}BM$ molecule had two clear absorption peaks at 605 and 353 nm. The main absorption band was in the range 300 to 800 nm, demonstrating strong absorption of visible light. The vertical lines indicate the oscillator strength of BT-$PC_{61}BM$, whereas the blue lines express the intramolecular electric charge transfer in $PC_{61}BM$ and the red lines express the intermolecular electric charge transfer between the BT molecule and $PC_{61}BM$ molecule. Furthermore, the intermolecular electric charge transfer occurs in the range 300 to 400 nm, and an absorption peak approximately 600 nm arises from the action of the BT molecule. Table 1 lists the vertical excitation energies and oscillator strengths for the thirty excited states, as calculated using the TDDFT method based on the optimized

States	Transition Energy (eV)[a]	f [b]	Δr(Å)[c]	Excited-state Property[d]
S_1	2.0506 (604.63 nm)	2.2006	0.759739	LE
S_2	2.4156 (513.27 nm)	0.0024	0.598960	LE
S_3	2.4404 (508.06 nm)	0.0467	0.419422	LE
S_4	2.4476 (506.55 nm)	0.0000	0.753877	LE
S_5	2.5183 (492.33 nm)	0.0001	3.497080	ICT
S_6	2.5328 (489.52 nm)	0.0006	4.502078	ICT
S_7	2.5382 (488.47 nm)	0.0006	5.387317	ICT
S_8	2.5523 (485.78 nm)	0.0000	1.796438	ICT
S_9	2.6739 (463.68 nm)	0.0001	0.178010	LE
S_{10}	2.6891 (461.06 nm)	0.0001	0.569387	LE
S_{11}	2.7191 (455.97 nm)	0.0004	0.619133	LE
S_{12}	2.7810 (445.83 nm)	0.0000	0.505284	LE
S_{13}	2.8326 (437.70 nm)	0.0000	0.199343	LE
S_{14}	2.8624 (433.15 nm)	0.0009	0.665378	LE
S_{15}	2.9473 (420.68 nm)	0.0014	0.706160	LE
S_{16}	2.9740 (416.90 nm)	0.0013	1.097320	LE
S_{17}	2.9945 (414.05 nm)	0.0000	0.601590	LE
S_{18}	3.0872 (401.61 nm)	0.0003	0.777263	LE
S_{19}	3.1032 (399.53 nm)	0.0026	0.735057	LE
S_{20}	3.1329 (395.75 nm)	0.0025	0.794401	LE
S_{21}	3.1703 (391.09 nm)	0.0081	0.158442	LE
S_{22}	3.2247 (384.49 nm)	0.0200	0.719405	LE
S_{23}	3.3056 (375.07 nm)	0.0000	7.582522	ICT
S_{24}	3.3712 (367.78 nm)	0.0006	7.344502	ICT
S_{25}	3.4619 (358.14 nm)	0.0012	0.338456	LE
S_{26}	3.5109 (353.14 nm)	0.2450	0.800606	LE
S_{27}	3.5121 (353.02 nm)	0.6954	1.791835	LE
S_{28}	3.5327 (350.96 nm)	0.0037	1.127917	LE
S_{29}	3.5501 (349.24 nm)	0.0005	6.733170	ICT
S_{30}	3.6982 (335.25 nm)	0.0013	0.230103	LE

Table 1. Selected electronic transition energies (eV) and corresponding oscillator strengths (*f*), main compositions and CI coefficients of the BT: $PC_{61}BM$ blend. [a]The numbers in parentheses are the transition energy wavelength. [b]Oscillator strength. [c]Δr index is a quantitative indicator of electron excitation mode, which is a measure of CT length. [d]$PC_{61}BM$ and BT in parentheses present the density are localized on the fullerene and polymer, respectively.

ground-state structure of the BT-$PC_{61}BM$ molecule, and these data also support our conclusion. The first four excited states of BT-$PC_{61}BM$ correspond to intramolecular electric charge transfer, whereas the fifth and sixth excitation states correspond to electric charge transfer between the BT molecule and the $PC_{61}BM$ molecule. In this study, we focused on the intermolecular electric charge transfer associated with the fifth and sixth excitation states.

The 3D real-space analysis method has been used to analyse the charge transfer in conjugated polymers because the charge difference density (CDD) determines the orientation and results of the charge transfer in molecular and molecular-metal systems[13]. As shown in Fig. 3, two types of excited state exist in the absorption band of BT-$PC_{61}BM$: one is the strong resonance charge transfer (CT) excited state, in which electron transfer occurs in the strong absorption region, and the other is weak resonance charge transfer. S_{22} and S_{23} are strong absorption excited states. S_{23} and S_{24} are pure intermolecular electric charge transfer excited states in which the electrons are mainly localized in the $PC_{61}BM$ molecule, and the holes are mainly localized in the main chain of the BT molecule, which demonstrates that electrons will be completely transferred from the BT molecule to the C_{60} molecule. S_4, S_5, S_6 and S_7 are weak absorption excited states. In the S_4 excited state, the electric charge is redistributed in the $PC_{61}BM$ molecule. The electrons and holes are mainly located in $C_{60,}$ which demonstrates that the S_4 excited state is

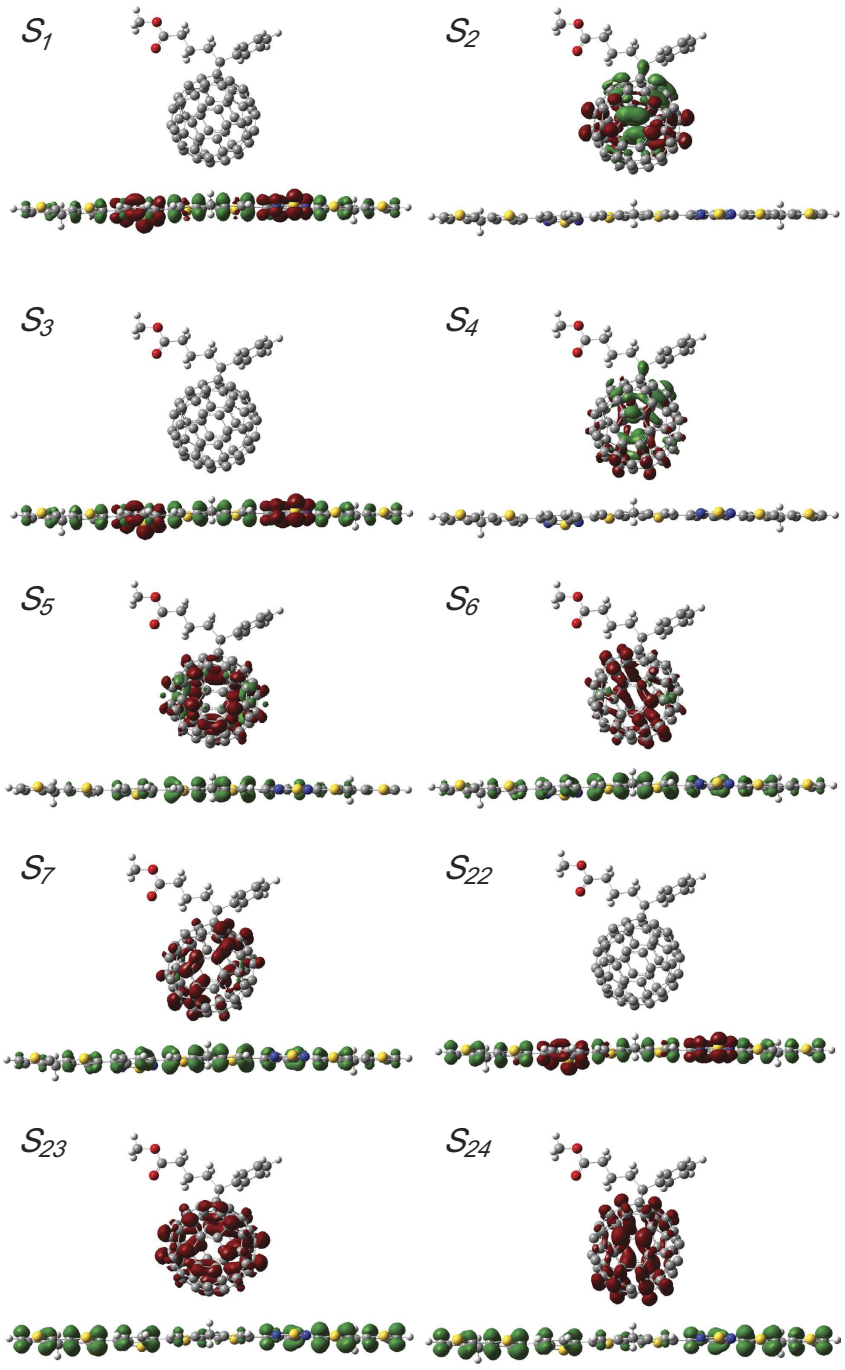

Figure 3. Selected charge difference densities (CDD) of the BT: $PC_{61}BM$ blend, in which the green and red colours represent the holes and electrons, respectively.

a localized excited (LE) state. For the S_5 and S_6 excited states, electrons are mainly transferred from the main chain of the BT molecule to C_{60}. However, states S_5 and S_6 are not pure intermolecular electric charge transfer excited states, as some of the holes are still located in C_{60}. Nevertheless, we are certain that S_5 and S_6 are the lowest intermolecular electric charge transfer states.

Figure 3 shows the qualitative visualization analysis with 3D charge difference density for charge transfer. To provide quantitative analysis of the charge transfer, Δr is introduced to measure charge-transfer length[18],

$$\Delta r = \frac{\sum_{ij}(K_i^j)^2 \left| \langle \varphi_j | r | \varphi_j \rangle - \langle \varphi_i | r | \varphi_i \rangle \right|}{\sum_{ij}(K_i^j)^2} \quad (1)$$

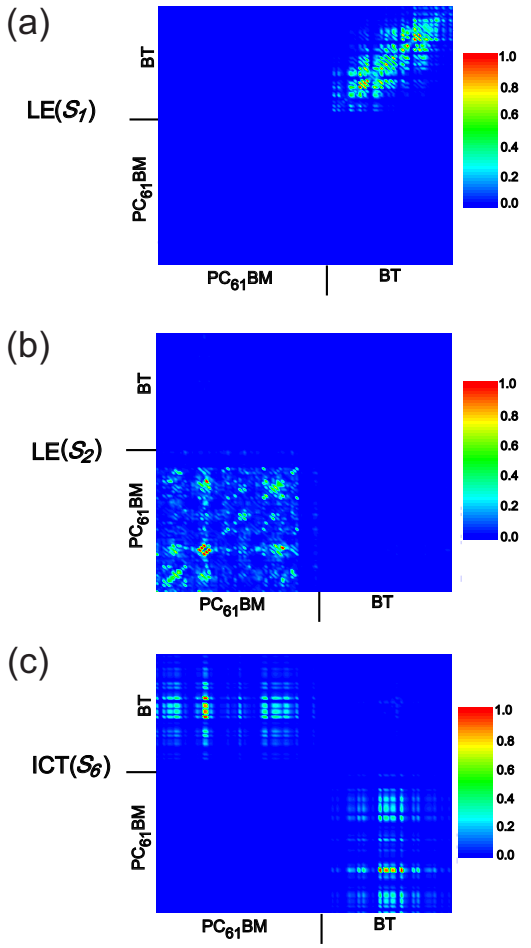

Figure 4. 2D site representation of transition density matrixes for S_1, S_2 and S_6. A colour scale bar is shown on the right.

where i and j traverse all of the occupied and virtual molecular orbitals, respectively, and φ is the orbital wave function. The larger Δr is the stronger charge transfer. The calculated results are summarized in Table 1, in which the S_5 and S_6 states have larger charge-transfer lengths, 3.497 Å and 4.502 Å, respectively. These calculations, along with the qualitative visualization analysis with 3D charge difference density, justify the previous conclusion that the excited-states S_5 and S_6 are the lowest intermolecular electric charge transfer states. The excited state *S7* (with *S6*) is degenerate and is also an intermolecular charge transfer excited state.

Charge difference density and Δr can be used to qualitatively and quantitatively analyse the charge transfer properties of the complex molecule in this study, but the electron-hole coherence on electronic transition cannot be demonstrated. In the two-dimensional (2D) site representation, photoexcitation creates an electron-hole pair or exciton by moving an electron from an occupied orbital to an unoccupied orbital. Each element of the transition density matrix reflects the dynamics of an exciton projected on a pair of atomic orbitals, indicated by indices, and increases the probability of finding one charged particle on site x and the second one on site y. The number of charged particles reflects the strength of the coherence between the donor and acceptor, which is defined by different colours of the element[15]. Figure 4 visualizes the electron-hole coherences, spatial span and primary sites of electron transitions. For S_1 and S_2, the electron-hole coherences are strong in the BT molecule and $PC_{61}BM$, respectively. They are the π-π^* transition of the inner donor and acceptor, as the electrons and holes are all localized in those units (see Fig. 4a,b). Therefore, S_1 and S_2 should be categorized as LE states. Furthermore, S_6 is an intermolecular charge transfer excited state owing to the electron and hole coherence between BT and $PC_{61}BM$. In other words, the electrons strongly cohere with holes between the the inner region of the BT molecules and the outer left region of PC61BM inner BT and left outer $PC_{61}BM$, but this coherence is weak between the the inner region of the BT molecule and the outer right region of PC61BM (see the 2D transition density matrix in Fig. 4c).

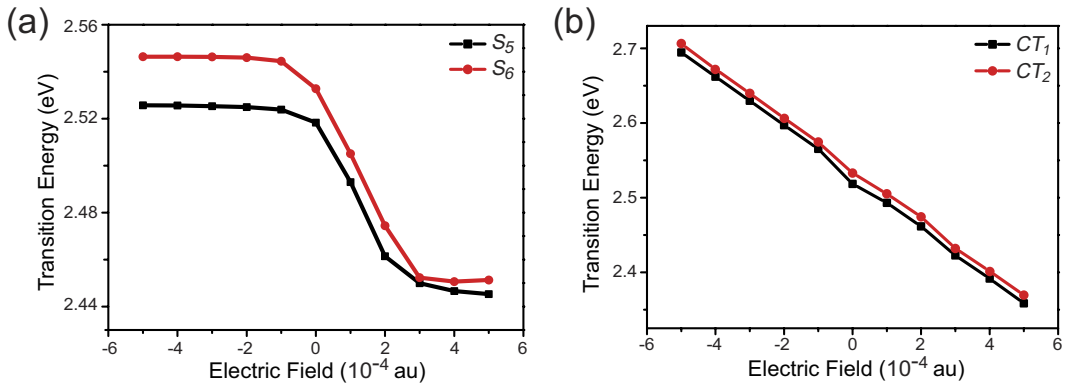

Figure 5. Excitation energy plotted against electric field strength for the lowest singlet excitation in $PC_{61}BM$-BT. The squares represent calculated values. The lines are fits to Eq. 9.

The charge transfer integral (electronic coupling matrix). The electronic coupling strength directly influences the electron transfer rate and determines the method of electron transfer. In this study, we used the generalized Mulliken-Hush (GMH) method to calculate the electronic coupling strength[19]. The expression is written as

$$V_{DA} = \frac{\mu_{tr}\Delta E}{\sqrt{(\Delta\mu)^2 + 4(\mu_{tr})^2}} \tag{2}$$

where μ_{tr} is the transition dipole moment, $\Delta\mu$ is the difference in the dipole moments between the S_0 and S_n states, and ΔE is the vertical excitation energy. $\Delta\mu$ can be obtained by the finite electric field method[20,21]. The external electric field $\boldsymbol{F}_{\text{ext}}$ is written as

$$\Delta E_{exc}(\mathrm{F}_{ext}) = \Delta E_{exc}(0) - \Delta\mu F_{ext} - \frac{1}{2}\Delta\alpha F_{ext}{}^2 \tag{3}$$

where $E_{exc}(0) = \Delta E = E_j - E_i$ is the excitation energy at the zero field and $\Delta\alpha$ is the polarizability. There is widespread consensus that hyperpolarizabilities can be simulated by using the quadratic response theory method. This approach was widely used for studying two-proton absorption (TPA) and to investigate the nonlinear optical (NLO) properties of nonlinear optical materials[22–27]. An experimental aspect, second harmonic generation (SHG), has been used to study photoinduced charge separation dynamics in organic semiconductor thin films using the time-resolved spectra technique. Some meaningful results have been obtained, including charge separation from a gradient in excitation density and differential electron/hole mobility in model systems of fullerene (C70) and semiconductor interfaces[28,29]. However, it is reasonable to believe that using quadratic response theory will not considerably affect our qualitative results for photoinduced charge transport efficiency controlled by external electric field. Therefore, the second harmonic generation (SHG) effect was not considered with the time-dependent density functional method. Figure 5 shows a nonlinear effect for S_5 and S_6, which are the lowest intermolecular electric charge transfer excited states. The data were obtained with the excited state electronic transitions energies calculation for the BT-$PC_{61}BM$ molecular system using the TDDFT method, and the difference in the dipole moments was obtained by fitting the calculated results of the S_5 and S_6 excited states with Eq. (3). Our calculations show the lowest intermolecular electric charge transfer state changes when we increase or decrease the external electric field. When the external electric field is $\boldsymbol{F}_{\text{ext}} = 1 \times 10^{-4}$ au, the lowest intermolecular electric charge transfer state is the S_5 or S_6 excited state. As the external electric field increases to 5×10^{-4} au, the lowest intermolecular electric charge transfer excited state changes to the S_2 or S_3 excited state. As the external electric field decreases to -5×10^{-4} au, the lowest intermolecular electric charge transfer excited state changes to the S_8 or S_9 excited state. We first visualized and analysed the excited states under different external electric fields to determine the lowest intermolecular electric charge transfer states; then, we determined the fit for the lowest intermolecular electric charge transfer states (see Fig. 5(b)). According to Eq. (3), the differences in dipole moment ($\Delta\mu$) for CT_1 and CT_2 are 12.4427 au and 12.4364 au, respectively. For the CT_1 excitation state, where μ_{tr} is 0.0300 au, the calculated V_{DA} is 0.0005 au. For the CT_2 excitation state, where μ_{tr} is 0.1000 au, the calculated V_{DA} is 0.0015 au.

Rate of exciton separation and electric charge recombination. The exciton separation and charge recombination are two separate excited-state processes, which compete with each other and together determine the photoelectric transformation efficiency of organic solar cells materials of equal

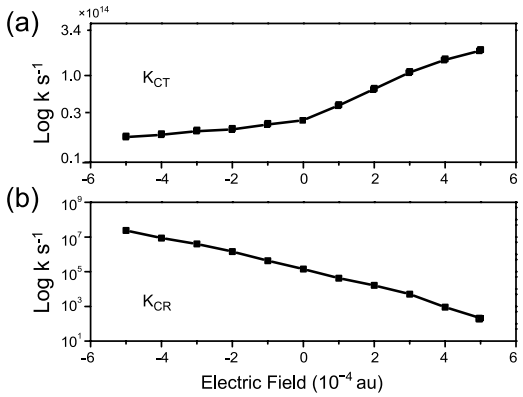

Figure 6. Calculated rate of exciton dissociation and charge recombination of the lowest ICT state of the $PC_{61}BM$: BT blend with different external electric fields based on Marcus theory.

importance. The free energy (ΔG) of exciton separation is expressed as ΔG_{CT}, and the free energy of electric charge recombination is expressed as ΔG_{CR}[30–36]. ΔG_{CR} is written as

$$\Delta G_{CR} = E_{IP}(D) - E_{EA}(A) \tag{4}$$

where E_{IP} *(D)* is the ionization potential of electrons in a donor and E_{EA} *(A)* is the ionization potential of holes in an acceptor. The calculated E_{IP} *(D)* and E_{EA} *(A)* are the energies of the highest occupied molecular orbital (HOMO) and lowest unoccupied molecular orbital (LUMO) of the donor and acceptor, respectively. These quantities are normally estimated from the geometry optimization of the isolated $PC_{61}BM$ adduct and BT by using the DFT method. The calculated ΔG_{CR} is −1.5060 eV. ΔG_{CT} can be obtained by the Rehm-Weller equation:

$$\Delta G_{CT} = -\Delta G_{CR} - \Delta E_{0-0} - E_b \tag{5}$$

where $\Delta E_{0\text{-}0}$ is the lowest excited state energy of a free radical donor and E_b is the exciton binding energy. The exciton binding energy is taken as the difference between the electronic and optical band gap energies. The electronic band gap can be approximated as the energy difference of HOMO and LUMO. The calculated E_b is 0.2685 eV and ΔG_{CT} is −0.7686 eV. The negative value of ΔG_{CT} means that electron transfer is thermodynamically favourable.

We used the Marcus model to calculate the rate of exciton separation and charge recombination, respectively. Figure 6(a) shows the calculated exciton separation rate for BT-$PC_{61}BM$. The exciton separation rate increases by one order of magnitude with the external electric field. According to the above calculations, the increase in exciton separation occurs due to the increase in ΔG_{CT} and λ_{CT} caused by the increase in the external electric field. From previous studies, we know that during the formation of the charge-separated state (D^+A^-), the Coulomb attraction pulls the charges back together to undergo first-order geminate recombination[37,38], that is the electron and hole may be trapped in each others' Coulomb well and forces the electric charge to recombine from the electric charge separation state at longer timescales. Also, this electric charge recombination process may occur again during exciton transport. As shown in Fig. 6(b), the change in the charge recombination rate calculated by the Marcus model with an external electric field is different from the exciton separation rate. The charge recombination rate decreases linearly with increases in the external electric field. By comparing Fig. 6(a,b), one can clear find that the initial CT dissociation rate is much larger than the recombination rate. And the relative slowness of the charge recombination rate originates from the vanishingly small electronic couplings and because recombination occurs deep in the inverted Marcus region ($|\Delta G_{CR}| = 1.5060\,\text{eV} \gg \lambda_{CR} = 0.4882\,\text{eV}$, at $\boldsymbol{F}_{ext} = 0$). Additionally, the charge recombination rate decreases by 6 orders when the external electric field changes from -5×10^{-4} au to 5×10^{-4} au, which is larger than exciton separation rate. The calculated charge separation rate variations are quite small for typical electric field values for organic solar cells. This result agrees with recent charge separation studies using time-resolved electric-field induced second harmonic generation[39]. The researchers concluded that the influence of the external field on the initial charge separation was minor and that the external electric field mainly influenced the charge collection via high carrier mobility in polymers[40].

Finally, the hot charge transfer exciton mechanism in organic photovoltaics may offer an alternative explanation for our computational results that the exciton separation rate is much higher than that of charge recombination[41]. The excess energy from charge separation results in a charge pair at an initial distance in the Coulomb potential. If this initial distance is longer than the critical escape distance, where the Coulomb binding energy is less than the thermal activation energy, charge separation occurs. Otherwise, the charge pair relaxes towards contact and probably eventual recombination[5]. For polymer/

fullerene interfaces, the excess energy of hot CT excitons may still play a role in assisting charge separation, even at sufficiently low temperatures[42]. This is mainly because hot CT excitons have relative weaker bonds from the Coulomb potential, and these excitons can be easier to dissociate. Electronic coupling from a donor exciton to a hot charge transfer exciton across the D/A interface can also be higher than the normal charge transfer expected from energy resonance. As a result, hole delocalization can further reduce the Coulomb attraction effect and accelerate the charge transfer process[43]. According to the results of our theoretical simulation on the BT-$PC_{61}BM$ complex, the calculated E_b is 0.2685 eV and ΔG_{CT} is −0.7686 eV respectively, excitons can sufficiently separate into electrons and holes at $\boldsymbol{F}_{ext}=0$ from the interfacial hot CT excitons perspective. Therefore, for this photoactive material in organic solar cells, the excitons separate into electrons and holes before they arrive at the donor-acceptor interface. ***But, according to our results, we must state that exciton dissociation is not the limiting factor in organic solar cells.*** Noted that, whether the interfacial energy gradient can overcome the Coulomb trap or not clearly should be system specific. These conclusions can greatly improve the photoelectric transformation efficiency of organic solar cells and decrease the loss of electrons in the transport process. Our findings are in accordance with a recent study revealing the enhanced probability of charge separation from highly delocalized hot interfacial charge transfer states[44], and provide an important design principle for new organic photovoltaics materials.

Discussion

In this study, the excited states of BT and $PC_{61}BM$ molecules were examined with a quantum-mechanical method. The BT-$PC_{61}BM$ complex has a broader spectrum response region than regular response regions, and strong absorption peaks are located in the visible light range. The lowest electric charge transfer state changes as the external electric field changes. The BT-$PC_{61}BM$ complex molecule has a high electric charge separation rate (3.1334×10^{13} s^{-1}) and a low electric charge recombination rate (1.4221×10^{5} s^{-1}) according to the Marcus model at $\boldsymbol{F}_{ext}=0$. After adding an external electric field, the charge recombination rate calculated with the Marcus model decreased linearly as the external electric field increased. The charge recombination rate decreased by 6 orders when the external electric field increased from -5×10^{-4} au to 5×10^{-4} au. The exciton separation rate increased with increases in the external electric field. The exciton separation rate is increased by one order. ***But, the exciton dissociation is not the limiting factor in organic solar cells according to our results.***

Methods

Charge transfer rate. For nonadiabatic and adiabatic reactions, the charge transfer is handled using different approximations. We chose the classic Marcus mode. In classic Marcus theory, Marcus proposed three assumptions about an adiabatic reaction: 1) The reactants have the same energy as the products, and the energy is conserved before and after the state-to-state transition; 2) The Frank-Condon principle is met; 3) The energy split is large, and the transition probability is 1 at the position of the transition state[45].

Exciton dissociation and charge recombination relate to the electron transition reaction. In the semi-classical limit from Marcus theory, the charge transfer rate is expressed as

$$k=\sqrt{\frac{4\pi^{3}}{h^{2}\lambda k_{B}T}}\,|V_{da}|^{2}\exp\left(-\frac{(\Delta G+\lambda)^{2}}{4\lambda k_{B}T}\right) \tag{6}$$

where k_B is the Boltzmann constant, h is Planck's constant, V_{da} is the electronic coupling between the initial and final states, λ is the reorganization energy, and T is the temperature ($T=300$ K).

Reorganization energy. The reorganization energy is an important parameter for characterizing the electron and energy transfer. According to the rate expression (Eq. (6)), the rate reaches its maximum value when the reorganization energy is at its minimum value[46–48]. In our research, we focused on the relationship between the inner reorganization energy and electron transfer. Before and after the electron transfer, the entire system will relax at a new steady state. The dissipative energy in the relaxation process is the reorganization energy. In other words, the reorganization energy is the relaxation energy. The reorganization energy is written as

$$\lambda=\lambda_{\mathrm{i}}+\lambda_{\mathrm{s}} \tag{7}$$

where λ_i is the internal reorganization energy arising from the change in equilibrium geometry of the donor and acceptor sites upon electron transfer and λ_s is the outer reorganization energy.

The inner reorganization energy consists of two sections[49,50]:

$$\lambda=\lambda_{1}(A)+\lambda_{2}(D) \tag{8}$$

$$\lambda_{1}(A)=E(A^{-})-E(A) \tag{9}$$

$$\lambda_2(D) = E(D) - E(D^+) \tag{10}$$

where $E(A^-)$ and $E(A)$ are the energies of the neutral acceptor A at the anion geometry and the optimal ground-state geometry, respectively, and $E(D)$ and $E(D^+)$ are the energies of the radical cation at the neutral geometry and optimal cation geometry. λ_s in Eq. (7) is the outer reorganization energy, which is related to the change in electronic and nuclear polarizations in electron transfer. The outer reorganization energy can be expressed as

$$\lambda_s = \frac{1}{8\pi\varepsilon_0}\left(\frac{1}{\varepsilon_{op}} - \frac{1}{\varepsilon_s}\right)\left(\frac{1}{R_D} + \frac{1}{R_A} - 2\sum_D\sum_A \frac{q_D q_A}{r_{DA}}\right) \tag{11}$$

where R_D and R_A are the radii of the donor and acceptor, respectively. q_D and q_A are the electric charge of the donor and acceptor, respectively. r_{DA} is the donor-acceptor distance. ε_0 is the dielectric constant in a vacuum. ε_{op} is the optical dielectric constant of the surrounding media and ε_s is the relative dielectric constant of the molecule[51–54].

Quantum chemical calculation method. BT and $PC_{61}BM$ were chosen as the photoactive materials for organic solar cells. All quantum chemistry calculations were performed by Gaussian 09 software[55]. The ground-state geometries of the BT-PC61BM molecule, isolated $PC_{61}BM$ adduct and BT were optimized using density functional theory (DFT)[56], the B3LYP functional[57,58], and the 6-31G(d) basis set. The molecular structures of isolated BT and $PC_{61}BM$ are shown in Fig. 1. To calculate the reorganization energies of the charge transfer reaction in Marcus theory, the cationic ground state geometry of isolated BT and the anionic ground state geometries of the isolated $PC_{61}BM$ adduct were also optimized with DFT, the B3LYP functional, and the 6-31G(d) basis set. Then, the single point energies of these two neutral acceptors at the anionic geometry and optimal ground-state geometry, as well as the single point energies of the radical cation at the neutral geometry and optimal cation geometry, were calculated at the same level of theory. Although previous theoretical studies have revealed that the conventional hybrid B3LYP functional could be sufficiently accurate for calculating charge transfer excited-states in some systems[59,60], the long-range-correction should be considered in quantum chemical calculations of large systems, such as the organic solar cell donor-acceptor heterojunction in this study[61]. Therefore, to simulate the optical absorption properties, a calculation of the excited state electronic transitions BT-$PC_{61}BM$ molecular system was performed using time-dependent density functional theory (TDDFT)[62], the long-range-corrected functional (CAM-B3LYP)[63], and the 6-31G(d) basis set. The long-range-corrected functional was employed for the non-Coulombic part of the exchange functional. Furthermore, geometry optimization of the lowest excited state of the isolated donor and the lowest excited state of the radical cation state was performed with TD-DFT, CAM-B3LYP, and the 6-31G (d) basis set. The *Generalized Mulliken-Hush* (GMH) model was employed to calculate the charge transfer integral (electronic coupling matrix). To investigate the effect of an external electric field on the excited-state properties of the molecules, the finite field method was employed, and the direction of the electric field is shown in Fig. 1. Fields ranging from -5×10^{-4} to 5×10^{-4} au were used. This result can be compared to the realistic strength of the electric field in the solar cell devices of up to 4×10^{-5} au ($\sim 2\times 107$ V/m). The field in a solar cell can be oriented in all possible directions. To visualize charge transfer during electronic transitions, two-dimensional (2D) site space analysis (transition density matrix) and three-dimensional (3D) real space analysis (charge difference density) were performed, which were described in detail in our previous article[13].

References

1. Gunes, S., Neugebauer, H. & Sariciftci, N. S. Conjugated Polymer-Based Organic Solar Cells. *Chem. Rev.* **107,** 1324–1338 (2007).
2. Rolczynski, B. S. *et al.* Ultrafast Intramolecular Exciton Splitting Dynamics in Isolated LowBand-Gap Polymers and Their Implications in Photovoltaic Materials Design. *J. Am. Chem. Soc.* **134,** 4142–4152 (2012).
3. Vandewal, K. *et al.* Efficient charge generation by relaxed charge-transfer states at organic interfaces. *Nat. mater.* **13,** 63–68 (2014).
4. Reed, A. E., Curtiss, L. A. & Weinhold, F. Intermolecular Interactions from a Natural Bond Orbital, Donor-Acceptor Viewpoint. *Chem. Rev.* **88,** 899–926 (1988).
5. Jailaubekov, A. E. *et al.* Hot charge-transfer excitons set the time limit for charge separation at donor/acceptor interfaces in organic photovoltaics. *Nat. Mater.* **12,** 66–73 (2013).
6. Chen, H. Y. *et al.* Polymer solar cells with enhanced open-circuit voltage and efficiency. *Nat. Photonics* **192,** 649–953 (2009).
7. Liang, Y. Y. *et al.* For the Bright Future—Bulk Heterojunction Polymer Solar Cells with Power Conversion Efficiency of 7.4%. *Adv. Mater.* **22,** 135–138 (2010).
8. Dou, L. *et al.* Tandem polymer solar cells featuring a spectrally matched low-bandgap polymer, *Nature Photonics* **6,** 180–185 (2012).
9. You, J. B. *et al.* A polymer tandem solar cell with 10.6% power conversion efficiency *Nat. Commun.* **4,** 1–10 (2013).
10. Marcus, R. A. & Sutin, N. Electron transfers in chemistry and biology, *Biochim. Biophys. Acta* **811,** 265–322 (1985).
11. Closs, G. L. & Miller, J. R. Intramolecular Long-Distance Electron Transfer in Organic Molecules. *Science* **240,** 440–447 (1988).
12. Closs, G. L., Calcaterra, L. T., Green, N. J. Penfiedld, K. W. & Miller, J. R. Distance, stereoelectronic effects, and the Marcus inverted region in intramolecular electron transfer in organic radical anions. *J. Phys. Chem.* **90,** 3673–3683 (1986).
13. Li, Y. Z., Pullerits, T., Zhao, M. Y. & Sun, M. T. Theoretical Characterization of the PC60BM:PDDTT Model for an Organic Solar Cell. *J. Phys. Chem. C* **115,** 21865–21873 (2011).

14. Song, P., Li, Z., Ma, F. C., Pullerits, T. & Sun, M. T. External Electric Field-Dependent Photoinduced Charge Transfer in a Donor–Acceptor System for an Organic Solar Cell. *J. Phys. Chem. C* **117,** 15879–15889 (2013).
15. Xia, L. X. *et al.* Visualized method of chemical enhancement mechanism on SERS and TERS. *J. Raman Spectrosc.* **45,** 533–540 (2014).
16. Stowell, M. H. B. *et al.* Light-Induced Structural Changes in Photosynthetic Reaction Center: Implications for Mechanism of Electron-Proton Transfer. *Science* **276,** 812–916 (1997).
17. Pattantyus-Abraham, A. G. *et al.* Depleted-Heterojunction Colloidal Quantum Dot Solar Cells. *ACS Nano*, **4,** 3374–3380 (2010).
18. Guido, C. A., Cortona, P., Mennucci, B. & Adamo, C. On the Metric of Charge Transfer Molecular Excitations: A Simple Chemical Descriptor. *J. Chem. Theory Comput.* **9,** 3118–3126 (2013).
19. Voityuk, A. A. Estimation of electronic coupling in-stacked donor-bridge-acceptorsystems: Correction of the two-state model. *J. Chem. Phys*. **124,** 064505 (2006).
20. Kjellberg, P., He, Z. & Pullerits, T. Bacteriochlorophyll in Electric Field. *J. Phys. Chem.* **107,** 13737–13742 (2003).
21. Grozema, F. C., Telesca, R., Jonkman, H. T., Siebbeles, L. D. A. & Snijders, J. G. Excited state polarizabilities of conjugated molecules calculated using time dependent density functional theory. *J. Chem. Phys*. **115,** 10014–10021 (2001).
22. Frediani, L., Ågren, H., Ferrighi, L. & Ruud, K. Second-harmonic generation of solvated molecules using multiconfigurational self-consistent-field quadratic response theory and the polarizable continuum model. *J. Chem. Phys*. **123,** 144117 (2005).
23. Foreman, B. A. Quadratic response theory for spin-orbit coupling in semiconductor heterostructures. *Phys. Rev. B* **72,** 165344 (2005).
24. Zhang, X. & Herbert, J. M. Analytic derivative couplings in time-dependent density functional theory: Quadratic response theory versus pseudo-wavefunction approach. *J. Chem. Phys*. **142** 064109 (2015).
25. Daya, P. N., Nguyen, K. A. & Pachter, R. Calculation of two-photon absorption spectra of donor-π-acceptor compounds in solution using quadratic response time-dependent density functional theory. *J. Chem. Phys.* **125,** 094103 (2006).
26. Ye, A. J. & Autschbacha, J. Study of static and dynamic first hyperpolarizabilities using time-dependent density functional quadratic response theory with local contribution and natural bond orbital analysis. *J. Chem. Phys.* **125,** 234101 (2006).
27. Rinkevicius, Z., Li, X., Sandberg, J. A. R. & Ågren, H. Non-linear optical properties of molecules in heterogeneous environments: a quadratic density functional/molecular mechanics response theory. *Phys. Chem. Chem. Phys.* **16,** 8981–8989 (2014).
28. Wu, X. X., Park, H. & Zhu, X. Y. Probing transient electric fields in photoexcited organic semiconductor thin films and interfaces by time-resolved second harmonic generation. *J. Phys. Chem. C* **118,** 10670–10676 (2014).
29. Nelson, C. A. *et al.* Time-, energy-, and phase-resolved second-harmonic generation at semiconductor interfaces. *J. Phys. Chem. C* **118,** 27981–27988 (2014).
30. Zhang, X. *et al.* Rational Design of d-PeT Phenylethynylated-Carbazole Monoboronic Acid Fluorescent Sensors for the Selective Detection of r-Hydroxyl Carboxylic Acids and Monosaccharides. *J. Am. Chem. Soc.* **131,** 17452–17463 (2009).
31. Norton, J. E. & Bredas, J. L. Polarization Energies in Oligoacene Semiconductor Crystals. *J. Am. Chem. Soc.* **130,** 12377–12384 (2008).
32. Liu, T., Cheung, D. L. & Troisi, A. Structural variability and dynamics of the P3HT/PCBM interface and its effects on the electronic structure and the charge-transfer rates in solar cellsw. *Phys. Chem. Chem. Phys*. **13,** 21461–21470 (2011).
33. Redmore, N. P., Rubtsov, I. V. & Therien, M. J. Synthesis, Electronic Structure, and Electron Transfer Dynamics of (Aryl) ethynyl-Bridged Donor-Acceptor Systems. *J. Am. Chem. Soc.* **125,** 8769–8778 (2003).
34. Imahori, H. *et al.* Stepwise Charge Separation and Charge Recombination in Ferrocene-meso, meso-Linked Porphyrin Dimer-Fullerene Triad. *J. Am. Chem. Soc.* **123,** 6617–6628 (2001).
35. Imahori, H. *et al.* Modulating Charge Separation and Charge Recombination Dynamics in Porphyrin-Fullerene Linked Dyads and Triads: Marcus-Normal versus Inverted Region. *J. Am. Chem. Soc*. **123,** 2607–2617 (2001).
36. Marcus, R. A. Electron Transfer Reactions in Chemistry: Theory and Experiment (Nobel Lecture). *Angew. Chem*. **32,** 1111–1121 (1993).
37. Pal, S. K. *et al.* Geminate charge recombination in polymer/fullerene bulk heterojunction films and implications for solar cell function. *J. Am. Chem. Soc.* **132,** 12440–12451 (2010).
38. Morteani, A. C., Sreearunothai, P., Herz, L. M., Friend, R. H. & Silva, C. Exciton regeneration at polymeric semiconductor heterojunctions. *Phys. Rev. Lett.* **92,** 247402 (2004).
39. Amarasinghe, V. D. *et al.* Visualizing charge separation in bulk heterojunction organic solar cells. *Nature Comm*. **4,** 2334 (2013).
40. Chen, M. *et al.* High carrier mobility in low band gap polymer-based field-effect transistors. *Appl. Phys. Lett.* **87,** 252105 (2005).
41. Zhu, X. Y., Yang, Q. & Muntwiler, M. Charge-transfer excitons at organic semiconductor surfaces and interfaces. *Acc. Chem. Res.* **42,** 1779–1787 (2009).
42. Lee, J. *et al.* Charge transfer state versus hot exciton dissociation in polymer_fullerene blended solar cells. *J. Am. Chem. Soc.* **132,** 11878–11880 (2010).
43. Bakulin, A. A. *et al.* The role of driving energy and delocalized states for charge separation in organic semiconductors. *Science* **335,** 1340–1344 (2012).
44. Grancini, G. *et al.* Hot exciton dissociation in polymer solar cells. *Nat. Mater.* **12,** 29–33 (2013).
45. Lemaur, V., Steel, M., Beljonne, D., Bredas, J. L. & Cornil, J. Photoinduced Charge Generation and Recombination Dynamics in Model Donor/Acceptor Pairs for Organic Solar Cell Applications: A Full Quantum-Chemical Treatment. *J. Am. Chem. Soc.* **127,** 6077–6086 (2005).
46. Bredas, J. L., Beljonne, D., Coropceanu, V. & Cornil, J. Charge-Transfer and Energy-Transfer Processes in π-Conjugated Oligomers and Polymers: A Molecular Picture. *Chem. Rev*. **104,** 4971–5004 (2004).
47. Deng, W. Q. & Goddard, W. A. Predictions of Hole Mobilities in Oligoacene Organic Semiconductors from Quantum Mechanical Calculations. *J. Phys. Chem. B* **108,** 8614–8621 (2004).
48. Coropceanu, V. *et al.* Charge Transport in Organic Semiconductors. *Chem. Rev*. **107,** 926–952 (2007).
49. Anthony, J. E. Functionalized Acenes and Heteroacenes for Organic Electronics. *Chem. Rev.* **106,** 5028–5048 (2006).
50. Guldi, D. M. Fullerene–porphyrin architectures; photosynthetic antenna and reaction center models. *Chem. Soc. Rev*. **31,** 22–36 (2002).
51. Norton, J. E. & Brédas, J. L. Polarization Energies in Oligoacene Semiconductor Crystals. *J. Am. Chem. Soc*. **2008,** 130, 12377.
52. McMahon, D. P. & Troisi, A. Evaluation of the External Reorganization Energy of Polyacenes. *J. Phys. Chem. Lett.* **1,** 941–946 (2010).
53. Seki, K., Traytak, S. D. & Tachiya, M. Rigorous calculation of electric field effects on the free energy change of the electron transfer reaction. *J. Chem. Phys*. **118,** 669 (2003).
54. Liu, T. & Troisi, A. Absolute Rate of Charge Separation and Recombination in a Molecular Model of the P3HT/PCBM Interface. *J. Phys. Chem. C* **115,** 2406–2415 (2011).
55. Frisch, M. J. *et al. Gaussian 09 Revision A.02*, Gaussian, Inc., Wallingford CT, (2009).
56. Hohenberg, P. & Kohn, W. Inhomogeneous electron gas. *Phys. Rev*. **136,** B864 (1964).
57. Becke, A. D. Density-functional exchange-energy approximation with correct asymptotic behaviour. *Phys. Rev. A* **38,** 3098 (1988).
58. Becke, A. D. Density-functional thermochemistry. III. The role of exact exchange. *J. Chem. Phys.* **98,** 5648 (1993).

59. Sun, M. T., Ding, Y. & Xu, H. X. Direct visual evidence for quinoidal charge delocalization in poly-p-phenylene cation radical. *J. Phys. Chem. B* **111,** 13266–13270 (2007).
60. Tretiak, S., Igumenshchev, K. & Chernyak, V. Exciton sizes of conducting polymers predicted by time-dependent density functional theory. *Phys. Rev. B* **71,** 033201 (2005).
61. Dreuw, A. & Head-Gordon, M. Failure of time-dependent density functional theory for long-range charge-transfer excited states: the zincbacteriochlorin–bacteriochlorin and bacteriochlorophyll–spheroidene complexes. *J. Am. Chem. Soc.* **126,** 4007–4016 (2004).
62. Gross, E. K. U. & Kohn, W. Local density-functional theory of frequency-dependent linear response. *Phys. Rev. Lett.* **55,** 2850 (1985).
63. Yanai, T., Tew, D. P. & Handy, N. C. A new hybrid exchange–correlation functional using the Coulomb-attenuating method (CAM-B3LYP). *Chem. Phys. Lett.* **393,** 51–57 (2004).

Acknowledgements

This work was supported by the National Natural Science Foundation of China (Nos. 91436102, 11474141 and 11374353), the Scientific Research Foundation for the Returned Overseas Chinese Scholars, State Education Ministry (Grant No. 2014-1685) and the Program of Liaoning Key Laboratory of Semiconductor Light Emitting and Photocatalytic Materials.

Author Contributions

M.S. and Y.Li. supervised the project, Y.F. and M.S. performed the calculations. M.S., Y.F. and Y.L. analysed the data and wrote the paper.

Additional Information

Competing financial interests: The authors declare no competing financial interests.

How to cite this article: Li, Y. *et al.* Photoinduced Charge Transport in a BHJ Solar Cell Controlled by an External Electric Field. *Sci. Rep.* **5**, 13970; doi: 10.1038/srep13970 (2015).

This work is licensed under a Creative Commons Attribution 4.0 International License. The images or other third party material in this article are included in the article's Creative Commons license, unless indicated otherwise in the credit line; if the material is not included under the Creative Commons license, users will need to obtain permission from the license holder to reproduce the material. To view a copy of this license, visit http://creativecommons.org/licenses/by/4.0/